J|A|C|S
ARTICLES
Published on Web 10/03/2002

Evidence for Single-Chain Magnet Behavior in a $Mn^{III}-Ni^{II}$ Chain Designed with High Spin Magnetic Units: A Route to High Temperature Metastable Magnets

Rodolphe Clérac,*,† Hitoshi Miyasaka,*,‡,§ Masahiro Yamashita,‡ and Claude Coulon†

Contribution from the Centre de Recherche Paul Pascal, CNRS UPR 8641, avenue du Dr. A. Schweitzer, 33600 Pessac, France, and "Structural Ordering and Physical Properties", PRESTO, Japan Science and Technology Corporation (JST) and Department of Chemistry, Graduate School of Science, Tokyo Metropolitan University, Minami-Ohsawa 1-1, Hachioji, Tokyo 192-0397, Japan

Received February 28, 2002

Abstract: We herein present the synthesis, crystal structure, and magnetic properties of a new heterometallic chain of Mn^{III} and Ni^{II} ions, $[Mn_2(saltmen)_2Ni(pao)_2(py)_2](ClO_4)_2$ (**1**) ($saltmen^{2-}$ = *N,N′*-(1,1,2,2-tetramethylethylene) bis(salicylideneiminate) and pao^- = pyridine-2-aldoximate). The crystal structure of **1** was investigated by X-ray crystallographic analysis: compound **1** crystallized in monoclinic, space group *C*2/*c* (No. 15) with $a = 21.140(3)$ Å, $b = 15.975(1)$ Å, $c = 18.6212(4)$ Å, $\beta = 98.0586(4)°$, $V = 6226.5(7)$ Å^3, and $Z = 4$. This compound consists of two fragments, the out-of-plane dimer $[Mn_2(saltmen)_2]^{2+}$ as a coordination acceptor building block and the neutral mononuclear unit $[Ni(pao)_2(py)_2]$ as a coordination donor building block, forming an alternating chain having the repeating unit $[-Mn-(O)_2-Mn-ON-Ni-NO-]_n$. In the crystal structure, each chain is well separated with a minimum intermetallic distance between Mn and Ni ions of 10.39 Å and with the absence of interchain π overlaps between organic ligands. These features ensure a good magnetic isolation of the chains. The dc and ac magnetic measurements were performed on both the polycrystalline sample and the aligned single crystals of **1**. Above 30 K, the magnetic susceptibility of this one-dimensional compound was successfully described in a mean field approximation as an assembly of trimers ($Mn\cdots Ni\cdots Mn$) with a $Ni^{II}\cdots Mn^{III}$ antiferromagnetic interaction ($J = -21$ K) connected through a ferromagnetic $Mn^{III}\cdots Mn^{III}$ interaction (J'). However, the mean field theory fails to describe the magnetic behavior below 30 K emphasizing the one-dimensional magnetic character of the title compound. Between 5 and 15 K, the susceptibility in the chain direction was fitted to a one-dimensional Ising model leading to the same value of J'. Hysteresis loops are observed below 3.5 K, indicating a magnet-type behavior. In the same range of temperature, combined ac and dc measurements show a slow relaxation of the magnetization. This result indicates the presence of a metastable state without magnetic long-range order. This material is the first experimental design of a heterometallic chain with $S_T = 3$ magnetic units showing a "single-chain magnet" behavior predicted in 1963 by R. J. Glauber for an Ising one-dimensional system. This work opens new perspectives for one-dimensional systems to obtain high temperature metastable magnets by combining high spin magnetic units, strong interunit interactions, and uniaxial anisotropy.

Introduction

Considerable efforts have been devoted to the synthesis of new magnetic systems in the nanometer size regime.[1] Motivation for this research stems from an interest in fundamental as well as applied aspects of nanomagnets. Researchers' main interests include reducing the magnetic unit dimensions in recording media to increase their capacity and testing the finite size effects predicted by theoretical models. Various physical approaches have been used to prepare single domain magnetic particles, but recently the preparation of high nuclearity magnetic clusters has revitalized this area of research in chemistry.[1b,2,3] Specifically, magnetic clusters such as $Mn_{12}O_{12}(O_2CR)_{16}(H_2O)_4$ compounds[2] exhibit a high spin ground state value ($S = 10$) and undergo a very slow relaxation of the magnetization below the so-called "blocking temperature" due to a negative uniaxial anisotropy ($D < 0$). These molecules are referred to as "single-molecule magnets" (SMM) and may be viewed as perfectly monodispersed superparamagnetic particles. The ability to prepare such "particles" is appealing for their aptitude to behave as a classical magnet on a purely molecular scale. Taking into

* To whom correspondence should be addressed. (R.C.) Fax: (+33) 5 56 84 56 00. E-mail: clerac@crpp.u-bordeaux.fr. (H.M.) Fax: (+81) 426 77 2525. E-mail: miyasaka@comp.metro-u.ac.jp.
† Centre de Recherche Paul Pascal.
‡ Tokyo Metropolitan University.
§ PRESTO, JST.

(1) (a) Thiaville, A.; Miltat, J. *Science* **1999,** *284*, 1939−1940 and references therein. (b) Gatteschi, D.; Caneschi, A.; Pardi, L.; Sessoli, R. *Science* **1994**, *265*, 1054−1058. (c) Leuenberger, M. N.; Loss, D. *Nature* **2001**, *410*, 789−793.

account the previous characteristics to obtain SMM, one idea would be to go one step further and synthesize "single-chain magnets" (SCM). To design this type of system, three essential ingredients need to be considered. First, spin carriers must exhibit a strong uniaxial anisotropy to be able to block or "freeze" their magnetization in one direction. The material also needs to exhibit a spontaneous magnetization to be called a magnet; individual magnetic moments in the chain then must not cancel out in the "frozen" state. Finally, chains must be isolated magnetically as much as possible to avoid tridimensional ordering. The occurrence of slow relaxation and Arrhénius behavior of the relaxation time in such systems was in fact already predicted using a one-dimensional Ising model in 1963 by R. J. Glauber.[4]

On the basis of these ideas, we have obtained a heterometallic one-dimensional system of Mn^{III} and Ni^{II} ions: $[Mn_2(saltmen)_2Ni(pao)_2(py)_2](ClO_4)_2$ (saltmen^{2-} = *N*,*N*′-(1,1,2,2-tetramethylethylene) bis(salicylideneiminate) and pao$^-$ = pyridine-2-aldoxime). We herein report the synthesis, X-ray crystal structure, and magnetic properties of this one-dimensional material exhibiting a single-chain magnet behavior. The first experimental evidence of single-chain magnet behavior confirming Glauber's prediction has been recently reported by A. Caneschi et al.[5] The compound $[Co^{II}(hfac)_2(NITPhOMe)]$ (hfac = hexafluoroacetylacetonate, NITPhOMe = 4′-methoxy-phenyl-4,4,5,5-tetramethylimidazoline-1-oxyl-3-oxide) has a spiral one-dimensional isolated chain structure. Because of the presence of anisotropic Co^{II} metal ions, this chain has been described as an Ising chain. As expected, detailed magnetic measurements of this compound show the occurrence of slow relaxation of the magnetization at low temperature. The results presented herein also confirm Glauber's prediction in a completely different chain system built with $S = 3$ trimer repeating units. The use of high spin magnetic units enhances the effective Ising exchange interaction in the chain and therefore opens a new route to the synthesis of metastable magnets at high temperature. Moreover, our work illustrates the universal dynamics of Ising-like chains.

Experimental Section

General Procedures and Materials. All chemicals and solvents used during the synthesis were reagent grade. The starting material $[Mn_2(saltmen)_2(H_2O)_2][ClO_4]_2$ was synthesized as described elsewhere.[6] The other building block $[Ni(pao)_2(py)_2]$ was prepared according to the literature method.[7] *Caution! Perchlorate salts are potentially explosive and should only be handled in small quantities.*

Preparation of 1. To a solution of $[Mn_2(saltmen)_2(H_2O)_2](ClO_4)_2$ (494 mg, 0.499 mmol) in 20 cm^3 of methanol was added a solution of $[Ni(pao)_2(py)_2]$ (459 mg, 1.000 mmol) in 20 cm^3 of methanol. After being stirred for 30 min at room temperature, the dark brown solution was diluted with 30 cm^3 of water. The resulting solution was filtered and allowed to stand for 2−3 days to form $[Mn_2(saltmen)_2Ni(pao)_2(py)_2](ClO_4)_2$ as dark brown crystals suitable for X-ray crystallography. They were collected by suction filtration, washed with a minimum amount of water, and dried in vacuo. Yield 86% (based on Mn). Anal. Calcd for $C_{62}H_{64}N_{10}O_{14}Cl_2Mn_2Ni$: C, 52.71; H, 4.57; N, 9.91. Found: C, 52.84; H, 4.41; N, 10.08. IR (KBr): ν(C≡N), 1601 cm^{-1}; ν(Cl−O), 1096, 1121, 1148 cm^{-1}.

Magnetic Measurements. Magnetic susceptibility measurements were obtained with the use of a Quantum Design SQUID magnetometer MPMS-XL. The dc measurements were collected from 1.8 to 300 K and from −50 to 50 kOe. The ac measurements were performed at various frequencies from 1 to 1500 Hz with an ac field amplitude of 3 Oe and no dc field applied. The data on the finely divided polycrystalline sample (46.93 mg) were corrected for the sample holder and for the diamagnetic contribution calculated from Pascal constants.[8] The data on a set of 13 aligned single crystals were normalized to the polycrystalline sample susceptibility above 80 K. Measurements were confirmed on three different polycrystalline samples and two other sets of oriented single crystals.

X-ray Data Collection, Reduction, and Structure Determination. Single crystals of **1** were prepared by the method described in the synthetic procedure. The single crystal for the crystallographic analysis was cut from a thin plate crystal and mounted on a glass rod. The crystal dimensions were 0.17 × 0.08 × 0.16 mm^3. Data collection was made on a Rigaku CCD diffractometer with graphite monochromated Mo Kα radiation (λ = 0.71069 Å) at a temperature of 20 ± 1 °C. An empirical absorption correction based on azimuthal scans of several reflections was applied. The data were corrected for Lorentz and polarization effects. The structure for **1** was solved by direct methods (SIR92)[9] and expanded using Fourier techniques.[10] The non-hydrogen atoms were refined anisotropically, while hydrogen atoms were introduced as fixed contributors. Full-matrix least-squares refinements based on 4539 observed reflections ($I > 3.00\sigma(I)$) were employed, where the unweighted and weighted agreement factors of $R1 = \sum||F_o| - |F_c||/\sum|F_o|$, $R2 = \sum(F_o^2 - F_c^2)/\sum F_o^2$, and $R_w = [\sum w(F_o^2 - F_c^2)^2/\sum w(F_o^2)^2]^{1/2}$ were used. The weighting scheme was based on counting statistics. Plots of $\sum w(F_o^2 - F_c^2)^2$ versus F_o^2, reflection order in data collection, sin θ/λ, and various classes of indices showed no unusual trends. Neutral atomic scattering factors were taken from Cromer and Waber.[11] Anomalous dispersion effects were included in F_c; the values $\Delta f'$ and $\Delta f''$ were those of Creagh and McAuley.[12] The values for the mass attenuation coefficients are those of Creagh and Hubbel.[13]

(2) Aubin, S. M. J.; Sun, Z.; Eppley, H. J.; Rumberger, E. M.; Guzei, I. A.; Folting, K.; Gantzel, P. K.; Rheingold, A. L.; Christou, G.; Hendrickson, D. N. *J. Am. Chem. Soc.* **2001**, *123*, 2127−2146. Christou, G.; Gatteschi, D.; Hendrickson, D. N.; Sessoli, R. *MRS Bull.* **2000**, *25*, 66−71. Aromi, G.; Aubin, S. M. J.; Bolcar, M. A.; Christou, G.; Eppley, H. J.; Folting, K.; Hendrickson, D. N.; Huffman, J. C.; Squire, R. C.; Tsai, H.-L.; Wang, S.; Temple, M. W. *Polyhedron* **1998**, *17*, 3005−3020. Barra, A.-L.; Brunel, L.-C.; Gatteschi, D.; Pardi, L.; Sessoli, R. *Acc. Chem. Res.* **1998**, *31*, 460−466. Friedman, J. R. *Phys. Rev. B* **1998**, *57*, 10291−10294. Sessoli, R.; Gatteschi, D.; Caneschi, A.; Novak, M. A. *Nature* **1993**, *365*, 141−143. Sessoli, R.; Tsai, H.-L.; Schake, A. R.; Wang, S.; Vincent, J. B.; Folting, K.; Gatteschi, D.; Christou, G.; Hendrickson, D. N. *J. Am. Chem. Soc.* **1993**, *115*, 1804−1816. Boyd, P. D. W.; Li, Q.; Vincent, J. B.; Folting, K.; Chang, H.-R.; Streib, W.; Huffman, J. C.; Christou, G.; Hendrickson, D. N. *J. Am. Chem. Soc.* **1988**, *110*, 8537−8539.

(3) Bouwen, A.; Caneschi, A.; Gatteschi, D.; Goovaerts, E.; Shoemaker, D.; Sorace, L.; Stefan, M. *J. Phys. Chem. B* **2001**, *105*, 2658−2663. Barra, A.-L.; Gatteschi, D.; Sessoli, R. *Chem.-Eur. J.* **2000**, *6*, 1608−1614. Goodwin, J. C.; Sessoli, R.; Gatteschi, D.; Wernsdorfer, W.; Powell, A. K.; Heath, S. L. *J. Chem. Soc., Dalton Trans.* **2000**, 1835−1840. Oshio, H.; Hoshino, N.; Ito, T. *J. Am. Chem. Soc.* **2000**, *122*, 12602−12603. Gatteschi, D.; Sessoli, R.; Cornia, A. *Chem. Commun.* **2000**, 725−732. Sangregorio, S.; Ohm, T.; Paulsen, C.; Sessoli, R.; Gatteschi, D. *Phys. Rev. Lett.* **1997**, *78*, 4645−4648.

(4) Glauber, R. J. *J. Math. Phys.* **1963**, *4*, 294−307.

(5) Caneschi, A.; Gatteschi, D.; Lalioti, N.; Sangregorio, C.; Sessoli, R.; Venturi, G.; Vindigni, A.; Rettori, A.; Pini, M. G.; Novak, M. A. *Angew. Chem., Int. Ed.* **2001**, *40*, 1760−1763. Caneschi, A.; Gatteschi, D.; Lalioti, N.; Sessoli, R.; Sorace, L.; Tangoulis, V.; Vindigni, A. *Chem.-Eur. J.* **2002**, *8*, 286−292. Caneschi, A.; Gatteschi, D.; Lalioti, N.; Sangregorio, C.; Sessoli, R.; Venturi, G.; Vindigni, A.; Rettori, A.; Pini, M. G.; Novak, M. A. *Europhys. Lett.* **2002**, *58*, 771−777.

(6) Miyasaka, H.; Clérac, R.; Ishii, T.; Chang, H.; Kitagawa, S.; Yamashita, M. *J. Chem. Soc., Dalton Trans.* **2002**, 1528−1534.

(7) Crause, R. A.; Busch, D. H. *J. Am. Chem. Soc.* **1960**, *82*, 4830−4834.

(8) Boudreaux, E. A.; Mulay, L. N. *Theory and Applications of Molecular Paramagnetism*; John Wiley & Sons: New York, 1976.

(9) SIR92: Altomare, A.; Burla, M. C.; Camalli, M.; Cascarano, M.; Giacovazzo, C.; Guagliardi, A.; Polidori, G. *J. Appl. Crystallogr.* **1994**, *27*, 435.

(10) DIRDIF94: Beurskens, P. T.; Admiraal, G.; Beurskens, G.; Bosman, W. P.; de Gelder, R.; Israel, R.; Smits, J. M. M. 1994.

(11) Cromer, D. T.; Waber, J. T. *International Tables for Crystallography*; The Kynoch Press: Birmingham, England, 1974; Vol. IV, Table 2.2A.

(12) Creagh, D. C.; McAuley, W. J. In *International Tables for Crystallography*; Wilson, A. J. C., Ed.; Kluwer Academic Publishers: Boston, 1992; Vol. C, Table 4.2.6.8, pp 219−222.

Table 1. Crystallographic Data for $[Mn_2(saltmen)_2Ni(pao)_2(py)_2](ClO_4)_2$ (**1**)

	1
formula	$C_{62}H_{64}N_{10}O_{14}Cl_2Mn_2Ni$
formula weight	1412.73
crystal system	monoclinic
space group	*C*2/*c* (No. 15)
T/°C	20 ± 1
λ/Å	0.71069
a/Å	21.140(3)
b/Å	15.975(1)
c/Å	18.6212(4)
α/°	90
β/°	98.0586(4)
γ/°	90
V/Å^3	6226.5(7)
Z	4
F_{000}	2920.00
μ(Mo Kα)/cm^{-1}	8.59
no. of reflections	7110
no. of observations ($I > 3.00\sigma(I)$)	4539
GOF	1.73
R1[a]	0.057
R2[b]	0.081
R_w[c,d]	0.063

[a] $R1 = \sum||F_o| - |F_c||/\sum|F_o|$. [b] $R2 = \sum(F_o^2 - F_c^2)/\sum F_o^2$. [c] $R_w = [\sum w(F_o^2 - F_c^2)^2/\sum w(F_o^2)^2]^{1/2}$. [d] $w = 1/[\sigma^2(F_o^2)]$.

All calculations were performed using the teXsan crystallographic software package of Molecular Structure Corp.[14] The crystal data and details of the structure determination for **1** are summarized in Table 1. Crystallographic data (excluding structure factors) for the structure reported in this paper have been deposited at the Cambridge Data Centre as supplementary publication no. CCDC-162777. Copies of the data can be obtained free of charge on application to CCDC, 12 Union Road, Cambridge CB21EZ, U.K. (fax, (+44) 1223-336-033; e-mail, deposit@ccdc.cam.ac.uk).

Results and Discussion

Formation of the Heterometallic Chain. $[Mn^{III}_2(saltmen)_2Ni^{II}(pao)_2(py)_2](ClO_4)_2$ was synthesized by the reaction of $[Mn^{III}_2(saltmen)_2(H_2O)_2](ClO_4)_2$ with $[Ni^{II}(pao)_2(py)_2]$ (where saltmen^{2-} is *N*,*N*′-(1,1,2,2-tetramethylethylene) bis(salicylideneiminate) and pao is pyridine-2-aldoximate) in a methanol/water mixed solution (Scheme 1). Dark brown crystals of **1** were obtained within 2−3 days in high yield. Although the assembly reaction of the starting materials was performed in a molar ratio of 1:2, that is, 1 equiv of $[Mn^{III}_2(saltmen)_2(H_2O)_2]^{2+}$ and 2 equiv of $[Ni^{II}(pao)_2(py)_2]$ (Mn:Ni = 1:1), the resulting compound **1** presents a 1:1 stoichiometry (Mn:Ni = 2:1). This result highlights the dimeric role of the $[Mn^{III}_2(saltmen)_2(H_2O)_2]^{2+}$ building block during the assembly process. This is in contrast with the classical idea that the manganese(III) salen-type Schiff base complexes are usually present in solution as an equilibrium between their monomeric $[Mn(SB)(S)_2]^+$ and dimeric species $[Mn_2(SB)_2(S)_2]^{2+}$ (SB, salen-type Schiff base ligand; S, unidentate solvent ligand). Thus, both species $[Mn(saltmen)(H_2O)(MeOH)]^+$ and $[Mn_2(saltmen)_2(H_2O)_2]^{2+}$ should be present in methanol during the formation of **1**. Nevertheless, as for the $[Mn_2(saltmen)_2(H_2O)_2](ClO_4)_2$ starting material, several other Mn(III) saltmen complexes with axial-capped ligands have shown an out-of-plane dimeric conformation ($[Mn_2(saltmen)_2(L)_2]^{0/2+}$ with L = the axial-capping ligand) in the solid state, even with longer plane-to-plane distance (for example, $[Mn_2(saltmen)_2(NCS)_2]$, Mn−O_{bridge} = 3.441(2) Å, and Mn···Mn = 4.0923(8) Å).[6] The synthesis of **1** seems to indicate that this family of Mn(III) complexes, crystallizing alone in a dimeric out-of-plane fashion, should be considered as a dimeric building block for the design of supramolecular architectures.

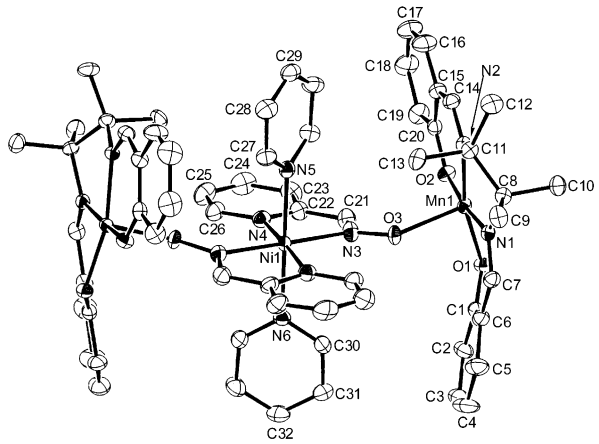

Figure 1. ORTEP drawing of the trinuclear cationic unit $[Mn_2(saltmen)_2Ni(pao)_2(py)_2]^{2+}$ of **1** with the atom numbering scheme of the unique atoms (30% probability ellipsoids).

Scheme 1

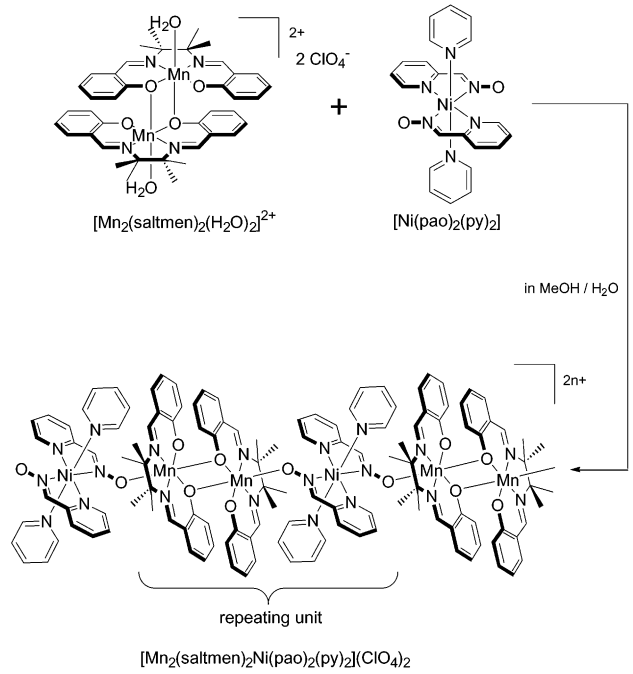

Structural Description. As shown Figure 1, X-ray crystallographic analysis revealed that the oximato group of the $[Ni^{II}(pao)_2(py)_2]$ monomeric species bridges the Mn^{III} dimers to form an alternating one-dimensional chain. Selected bond distances and angles with their estimated standard deviations are given in Table 2.

The Ni^{II} ion of the $[Ni(pao)_2(py)_2]$ moiety occupies the inversion center with a two-fold axis. The geometry of the Ni^{II} ion is a slightly distorted octahedron. The in-plane positions are occupied by two pao *N*,*N*-bidentate ligands with bond distances of Ni(1)−N(3) = 2.063(4) Å and Ni(1)−N(4) =

(13) Creagh, D. C.; Hubbell, J. H. In *International Tables for Crystallography*; Wilson, A. J. C., Ed.; Kluwer Academic Publishers: Boston, 1992; Vol. C, Table 4.2.4.3, pp 200−206.
(14) teXsan: Crystal Structure Analysis Package, Molecular Structure Corp. (1985 and 1992).

Table 2. Relevant Bond Distances (Å) and Angles (deg) for $[Mn_2(saltmen)_2Ni(pao)_2(py)_2](ClO_4)_2$ (**1**) with the Estimated Standard Deviations in Parentheses

Ni(1)−N(3)	2.063(4)	Mn(1)−O(1)	1.910(3)
Ni(1)−N(3)[a]	2.063(4)	Mn(1)−O(1)[b]	2.551(3)
Ni(1)−N(4)	2.106(4)	Mn(1)−O(2)	1.870(3)
Ni(1)−N(4)[a]	2.106(4)	Mn(1)−O(3)	2.116(3)
Ni(1)−N(5)	2.150(5)	Mn(1)−N(1)	1.988(3)
Ni(1)−N(6)	2.149(5)	Mn(1)−N(2)	1.981(3)
N(3)−O(3)	1.328(5)	Mn(1)···Mn(1)[b]	3.416(1)
N(3)−Ni(1)−N(3)[a]	178.4(2)	O(1)−Mn(1)−O(1)[b]	81.1(1)
N(3)−Ni(1)−N(4)	77.8(2)	O(1)−Mn(1)−O(2)	93.3(1)
N(3)−Ni(1)−N(4)[a]	102.2(2)	O(1)−Mn(1)−O(3)	90.9(1)
N(3)−Ni(1)−N(5)	89.2(1)	O(1)−Mn(1)−N(1)	91.3(1)
N(3)−Ni(1)−N(6)	90.8(1)	O(1)−Mn(1)−N(2)	166.1(1)
N(4)−Ni(1)−N(4)[a]	176.1(2)	O(1)−Mn(1)−O(2)[b]	82.0(1)
N(4)−Ni(1)−N(5)	92.0(1)	O(1)−Mn(1)−O(3)[b]	171.9(1)
N(4)−Ni(1)−N(6)	88.0(1)	O(1)−Mn(1)−N(1)[b]	93.5(1)
N(5)−Ni(1)−N(6)	180	O(1)−Mn(1)−N(2)[b]	87.5(1)
Ni(1)−N(3)−O(3)	123.9(3)	O(2)−Mn(1)−O(3)	98.4(1)
N(3)−O(3)−Mn(1)	131.8(2)	O(2)−Mn(1)−N(1)	173.0(1)
Mn(1)−O(1)−Mn(1)[a]	98.9(1)	O(2)−Mn(1)−N(2)	92.9(1)
N(1)−Mn(1)−N(2)	81.5(1)	O(3)−Mn(1)−N(1)	86.8(1)
		O(3)−Mn(1)−N(2)	100.5(1)

[a] Symmetry operation: $-x+1, y, -z+{}^1/_2$. [b] Symmetry operation: $-x+{}^1/_2, -y+{}^1/_2, -z$.

2.106(4) Å, and the axial positions are occupied by two pyridine unidentate ligands with bond distance of Ni(1)−N(5) = 2.150(5) Å. The oximato group of the $[Ni(pao)_2(py)_2]$ moiety bridges to the Mn^{III} ion of the $[Mn_2(saltmen)_2]^{2+}$ dimer with bond distances of Mn(1)−O(3) = 2.116(3) Å, N(3)−O(3) = 1.328(5) Å and angles of Mn(1)−O(3)−N(3) = 131.8(3)°, Ni(1)−N(3)−O(3) = 123.9(3)°. The Mn sites assume a square bipyramidal six-coordination geometry (out-of-plane dimeric fashion). The two apical positions are occupied by phenolate oxygen O(1)[a] arising from the neighboring $[Mn(saltmen)]^+$ moiety (Mn(1)−O(1)[a] = 2.551(3) Å, Mn(1)−O(1)−Mn(1)[a] = 98.9(1)°, O(1)−Mn(1)−O(1)[a] = 81.1(1)°, and Mn(1)···Mn(1)[a] = 3.416(1) Å with *a* as $1-x, y, {}^1/_2-z$) and oximato oxygen O(3) arising from the $[Ni(pao)_2(py)_2]$ moiety.[15] The bond distances around the Mn site are longer with the apical oxygens O(3) and O(1)[a] than with the equatorial sites occupied by the set of N(1), N(2), O(1), O(2) donor atoms of the $saltmen^{2-}$ quadridentate ligand (equatorial average bond distances: ⟨Mn−N⟩ = 1.985(3) Å and ⟨Mn−O⟩ = 1.890(3) Å). Therefore, the coordination sphere of the Mn(III) metal ion can be viewed as strongly distorted along the apical O(3)Mn(1)O(1)[a] direction also parallel to the chain axis. Figure 2 shows a packing diagram of **1**. Each chain runs in the *ac* plane and is separated from the nearest chains with a minimum intermetallic distance between Mn and Ni of 10.39 Å. It is also important to note for the following discussion of the magnetic properties that no significant interchain π stacking is observed between the phenyl rings of the saltmen ligand.

Magnetic Properties. Magnetic measurements were first performed on a polycrystalline sample of the Mn_2Ni chain between 300 and 1.8 K. Upon cooling, the inverse of the dc susceptibility ($1/\chi$, where $\chi = M/H$) decreases linearly from 300 to 120 K following roughly a Curie−Weiss behavior with $C =$ 6.8 emu·K/mol and $\theta = -26$ K (Figure 3). The Curie constant is in good agreement with the expected spin-only value of 7 emu·K/mol for two Mn^{III} ($S = 2$) and one Ni^{II} ($S = 1$), taking into account an average *g* value of 2. The slightly lower value of *C* could be explained by an average *g* value of 1.97 or due to a small extrinsic diamagnetic contribution. The Weiss constant sign indicates that the dominant interaction between spin carriers is antiferromagnetic.[16] As the magnetic interaction in similar dimeric building blocks of Mn^{III} is relatively small and ferromagnetic (ca. less than +3 K),[6,15,17] it is easy to conclude that the Ni^{II}···Mn^{III} interaction (*J*) is antiferromagnetic and much larger than the intrachain Mn^{III}···Mn^{III} interaction (*J′*) and the

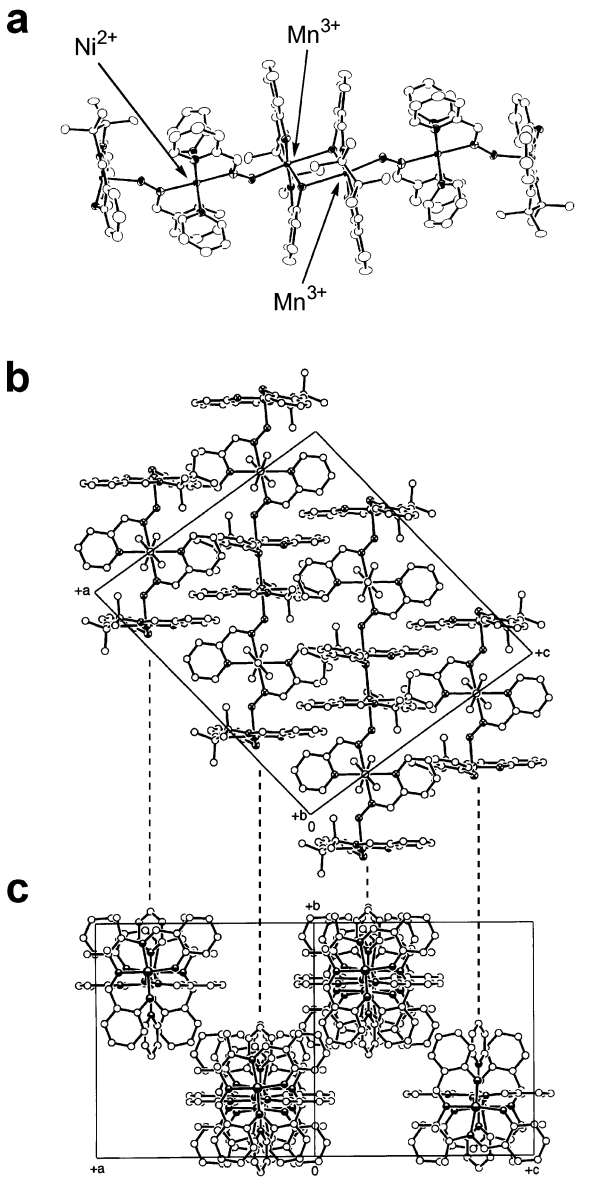

Figure 2. Views of the crystal structure of $[Mn_2(saltmen)_2Ni(pao)_2(py)_2](ClO_4)_2$ (**1**) showing (a) the heterometallic chain, (b) the projection in the *ac* plane where the chain is running, and (c) the projection along the chain axis. Perchlorate ions located between chains are omitted for clarity.

(15) The core geometry of the out-of-plane dimeric fragment is similar to what is found in the starting material $[Mn_2(saltmen)_2(H_2O)_2](ClO_4)_2$ ($Mn-O_{bridge}$ = 2.434(2) Å, Mn−O−Mn = 101.58(10)°, $O_{bridge}-Mn-O_{bridge}$ = 78.42(10)°, Mn···Mn = 3.381(1) Å) which exhibits ferromagnetic exchange interaction (J_{Mn-Mn}/k_B = +2.6 K) between Mn(III) ions via phenolate oxygen (see ref 6).

(16) The zero field splitting term (*D*) is negligible as compared to the magnetic interactions in this system. The *D* value is usually less than 5 K for comparable Mn^{III} and Ni^{II} systems. Quantitatively, the Weiss constant of −26 K is weakly affected by this contribution.

(17) Sato, Y.; Miyasaka, H.; Matsumoto, N.; Okawa, H. *Inorg. Chim. Acta* **1996**, *247*, 57−63. Shyu, H.-L.; Wei, H.-H.; Wang, Y. *Inorg. Chim. Acta* **1999**, *290*, 8−13.

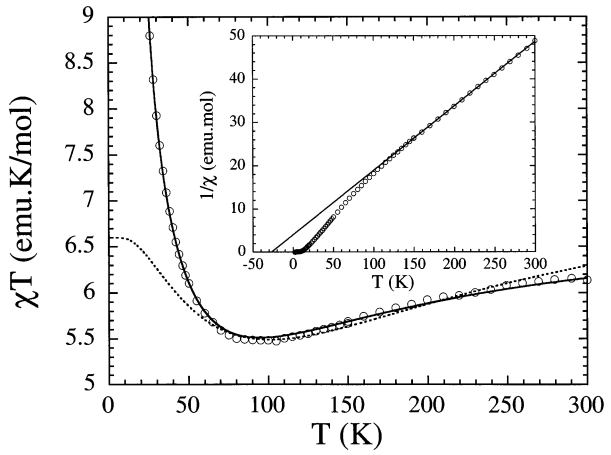

Figure 3. Temperature dependence of the χT product (where $\chi = M/H$) at 1000 Oe above 30 K measured on a polycrystalline sample of **1**. Dotted and solid lines correspond to the best fits obtained with a trimer Mn···Ni···Mn model and the mean field approximation for a chain of trimers, respectively (see text). Inset: Temperature dependence of the $1/\chi$ at 1000 Oe between 1.8 and 300 K. Solid line corresponds to the best fit obtained with the Curie−Weiss law above 120 K.

Table 3. Energy and Degeneracy of the Spin States of the Mn^{III}···Ni^{II}···Mn^{III} Trimer in Zero Field Sorted by Increasing Energy

			spin degeneracy		
i	S_{2Mn}	S_T	$(2S_T+1)$	$S_T(S_T+1)$	$-(E_i-8J)/J$
1	4	3	7	12	0
2	3	2	5	6	2
3	2	1	3	2	4
4	1	0	3	0	6
5	4	4	9	20	8
6	3	3	7	12	8
7	2	2	5	6	8
8	1	1	3	2	8
9	0	1	1	2	10
10	1	2	5	6	12
11	2	3	7	12	14
12	3	4	9	20	16
13	4	5	11	30	18

possible weak interchain (J'') coupling (the lastest, being due to weak π overlaps of aromatic rings, is most likely antiferromagnetic). From this point of view, the material looks like an assembly of trimers (Mn···Ni···Mn) with Ni^{II}···Mn^{III} antiferromagnetic interactions (J) connected through weak J' and J'' interactions. The first attempt to model the magnetic susceptibility was done with a simple Mn^{III}···Ni^{II}···Mn^{III} trimer model (neglecting J' and J''), based on the following Heisenberg Hamiltonian and assuming a external magnetic field H along the z axis ($H = H_z$):

$$\mathscr{H} = -2J\{\mathbf{S}_{Mn1}\cdot\mathbf{S}_{Ni} + \mathbf{S}_{Ni}\cdot\mathbf{S}_{Mn2}\} + g\mu_B S_{Tz} H_z \qquad (1)$$

where $\boldsymbol{S}_T$ is the total spin operator of the trimer with $\boldsymbol{S}_T = \boldsymbol{S}_{Mn1} + \boldsymbol{S}_{Ni} + \boldsymbol{S}_{Mn2}$, S_{Tz} is the z component of the $\boldsymbol{S}_T$ operator, and g is the Landé factor assuming $g = g_{Ni} = g_{Mn}$. The Hamiltonian (1) also reads:

$$\mathscr{H} = -J\{\mathbf{S}_T^2 - \mathbf{S}_{Ni}^2 - \mathbf{S}_{2Mn}^2\} + g\mu_B S_{Tz} H_z \qquad (2)$$

where $\boldsymbol{S}_{2Mn} = \boldsymbol{S}_{Mn1} + \boldsymbol{S}_{Mn2}$. The diagonalization of $\mathscr{H}$ leads to 13 different eigenvalues E_i (Table 3) which can be calculated from eq 3:

$$E_i = -J[S_T(S_T+1) - S_{2Mn}(S_{2Mn}+1) - S_{Ni}(S_{Ni}+1)] + g\mu_B H_z m_s \qquad (3)$$

where m_s are the eigenvalues of S_{Tz}.

From these energy levels, the magnetic susceptibility can be easily calculated in the $\mu_B H/k_B T \ll 1$ approximation by the Van Vleck equation.[18]

As shown in Figure 3, this isolated trimer model reproduces the experimental data above 50 K with $J/k_B = -30.0(5)$ K and $g = 2.09(2)$ (see Figure 3, dotted line). However, a strong increase of the χT product below 50 K is observed, which reveals the presence of ferromagnetic intertrimer magnetic couplings. As a first approach, these weak interactions were included in the model and treated in a mean field theory. Our main goal is to compare the experimental result with the prediction of this approach as it is the most convincing way to probe the anisotropy of the intertrimer interactions.[19] In this approximation, the magnetic susceptibility expression becomes:

$$\chi = \frac{\chi_{trimer}}{1 - \dfrac{4J_i}{Ng^2\mu_B^2}\chi_{trimer}} \qquad (4)$$

where $J_i = J' + 4J''$ as each trimer is surrounded by two trimers within a chain and by eight trimers on neighboring chains (see Figure 2). This expression gives a good agreement with the experimental data above 30 K. The best set of parameters obtained is $J/k_B = -21.0(1)$ K, $J_i/k_B = +0.7(1)$ K, and $g = 1.97(1)$ (solid line, Figure 3). The effective magnetic interaction (J_i) is ferromagnetic, indicating that J' is the dominant intertrimer interaction. The calculated parameters, physically acceptable regarding the proposed model, are in good agreement with the Curie−Weiss fit mentioned above.

As shown in Figure 4, a divergence of the susceptibility is predicted at 10.7 K by expression (4). This value is an underestimation of the mean field transition temperature (T_{MF}) as the expected three-dimensional order is antiferromagnetic (J'' is negative). In the case of isotropic interactions ($J' \approx |J''|$), the mean field theory would lead to reasonable estimation of the real critical temperature.[20] Therefore, an antiferromagnetic phase transition would occur around 10 K. This behavior is not observed experimentally, and a large deviation from mean field

(18) The Van Vleck equation reads:

$$\chi = \frac{N\sum_{i=1}^{n}(g\mu_B m_{si})^2 \exp(-E_i^{(0)}/k_B T)}{k_B T \sum_{i=1}^{n}\exp(-E_i^{(0)}/k_B T)}$$

where $E_i^{(0)}$ is the energy of the i state in zero field, and N is the number of trimer. An analytical expression of the magnetic susceptibility can then be proposed:

$$\chi_{trimer} = 2Ng^2\mu_B^2/k_B T\,[55e^{18J/k_BT} + 30e^{16J/k_BT} + 14e^{14J/k_BT} + 5e^{12J/k_BT} + e^{10J/k_BT} + 50e^{8J/k_BT} + e^{4J/k_BT} + 5e^{2J/k_BT} + 14]/[11e^{18J/k_BT} + 9e^{16J/k_BT} + 7e^{14J/k_BT} + 5e^{12J/k_BT} + 3e^{16J/k_BT} + 24e^{8J/k_BT} + e^{6J/k_BT} + 3e^{4J/k_BT} + 5e^{2J/k_BT} + 7]$$

(19) Chaikin, P. In *Review of the Physics of Low Dimensional Systems*; Miller, J. S., Epstein, A. J., Eds.; Annals of the New York Academy of Science: New York, 1978; Vol. 313, pp 129−144.

(20) Domb, C. In *Ising Model*; Domb, C., Green, M. S. Eds.; Academic Press: London, 1974; Vol. 3, p 425.

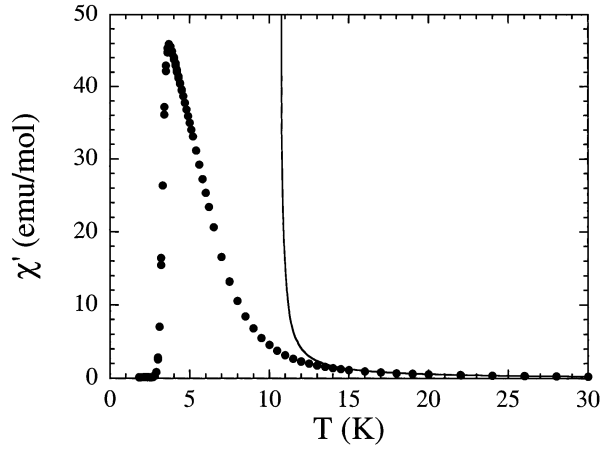

Figure 4. Temperature dependence of the susceptibility χ' (where $\chi' = dM/dH$) on a polycrystalline sample of **1** in zero external magnetic field, in a 3 Oe ac field, at 1 Hz from 1.8 to 7 K, and 125 Hz above 7 K where χ' is independent of the ac frequency. The solid line is the mean field fit discussed in the text and shown in Figure 3.

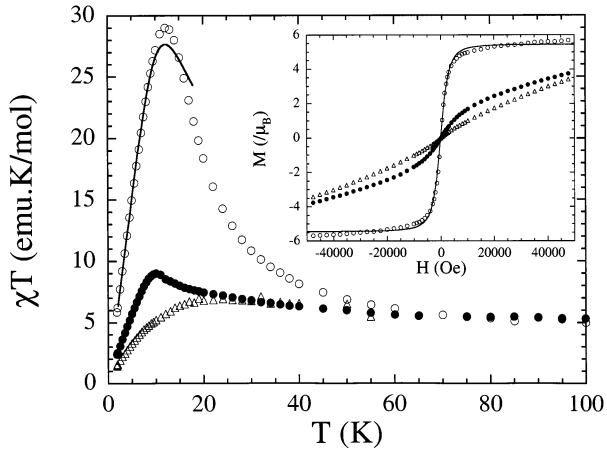

Figure 5. Magnetic measurements on oriented single crystals of **1** along the chains (○) perpendicular to the chains in the *ac* plane (●) and along the monoclinic *b* axis (△). Temperature dependence of the χT product (where $\chi = M/H$) at 10 kOe below 100 K; the solid line corresponds to the best fits obtained with the one-dimensional Ising model (see text). Inset: Field dependence of the magnetization at 10 K. The solid line corresponds to the best fit obtained with the one-dimensional Ising model.

is found at low temperature (see Figure 4). This result emphasizes the anisotropy of the intertrimer interactions ($J' \gg |J''|$) and the one-dimensional nature of the system as suggested by the structural studies.

Moreover, the susceptibility shown in Figure 4 exhibits a sharp maximum around 3.5 K, at a much lower temperature than T_{MF}. To discuss in more detail the nature of the paramagnetic phase above 3.5 K, we have performed additional experiments on oriented single crystals in three perpendicular directions including the monoclinic *b* axis (Figure 5).

Below 60 K, the susceptibility becomes anisotropic and reveals above 20 K a quasi uniaxial symmetry.[21] This implies that the chain axis, where the maximum of the magnetic response is measured, is close to the easy axis. This conclusion is in agreement with the geometry of the coordination sphere of Mn^{III} metal ions, which present a uniaxial (Jahn−Teller) distortion along the chain axis. This anisotropy is confirmed by the field dependence of the magnetization (for example, at 10 K, see inset of Figure 5), which quickly saturates when the field is applied along the chain direction, at $6\mu_B$ per trimer (expected value for an antiferromagnetically coupled $Mn^{III}\cdots Ni^{II}\cdots Mn^{III}$ trimer). To model these results, this anisotropy should be taken into account. The simplest relevant approach is a one-dimensional Ising model which also implies that each trimer can be described as a two states unit. As shown in Figure 3, this is the case below 20 K as χT, for the noninteracting trimer model, saturates to the value expected for an $S_T = 3$ system. This is consistent with Table 3, which indicates that only the seven $S_T = 3$ spin states are populated at low temperature. The degeneracy of these states is removed in the presence of magnetic anisotropy (zero field splitting, $\mathcal{H}_a = D\sum_i S_{Tzi}^2$). Therefore, all of the corresponding energy levels should to be taken into account to modelize the magnetization, for example, in a transfer matrix calculation. We have used a simplified treatment which consists of keeping only the two $S_z = \pm 3$ spin states.[22] At this approximation, the Hamiltonian reads:

$$\mathcal{H} = -2J' \sum_i S_{Tzi} S_{Tz(i+1)} + g\mu_B H_z \sum_i S_{Tzi} \qquad (5)$$

To identify this expression to the one-dimensional Ising Hamiltonian, one should introduce $\sigma_i = -S_{Tzi}/3$ (with $\sigma_i = \pm 1$). Therefore, using Glauber's notation, expression (5) becomes:

$$\mathcal{H} = -J'_{eff} \sum_i \sigma_i \sigma_{i+1} - \mu_{eff} H \sum_i \sigma_i \qquad (6)$$

with $J'_{eff} = 18J'$ and $\mu_{eff} = 3g\mu_B \approx 6\mu_B$. This model[23] gives the magnetization as the function of the temperature and the magnetic field:

$$M = N\mu_{eff} \frac{\sinh\left(\frac{\mu_{eff}H}{k_B T}\right)}{\sqrt{\sinh^2\left(\frac{\mu_{eff}H}{k_B T}\right) + \exp\left(\frac{-4J'_{eff}}{k_B T}\right)}} \qquad (7)$$

The expression has been used to fit the data between 5 and 15 K (solid lines in Figure 5 and its inset). The obtained parameters are $\mu_{eff}/\mu_B = 5.4$ and $J'_{eff}/k_B = +12$ K. The first one is consistent with the expected moment at saturation $\mu_{eff}/\mu_B = 6$, and the later gives $J' = +0.67$ K, in agreement with the value previously estimated from the mean field model. It worth noticing that the rapid saturation of the magnetization along the chain (inset of Figure 5) is compatible with one-dimensional correlations and does not imply a long-range magnetic order. Above 15 K, the theoretical model will be more complicated due to the population of the trimer excited states and to the necessary crossover toward a Heisenberg behavior described previously.

In the low temperature region, below 3.5 K, the magnetic studies reveal new interesting features. As shown in Figure 6, hysteresis loops are observed at 1.8 K in the three main directions with an orientation-dependent shape. This anisotropy is reminiscent of the one observed at higher temperature (see inset of Figure 5). Along the chain axis, as already mentioned

(21) The weak anisotropy which appears below 20 K in the plane perpendicular to the chains may be real or the consequence of a misorientation of the crystals.
(22) Strictly speaking, this approximation is valid for $D < 0$ and $k_B T \ll -5D$, which is a reasonable treatment in our system below 15 K.
(23) Thompson, C. J. *Phase Transition and Critical Phenomena*; Domb, C., Green, M. S., Eds.; Academic Press: London, 1972; Vol. 1, pp 177−226.

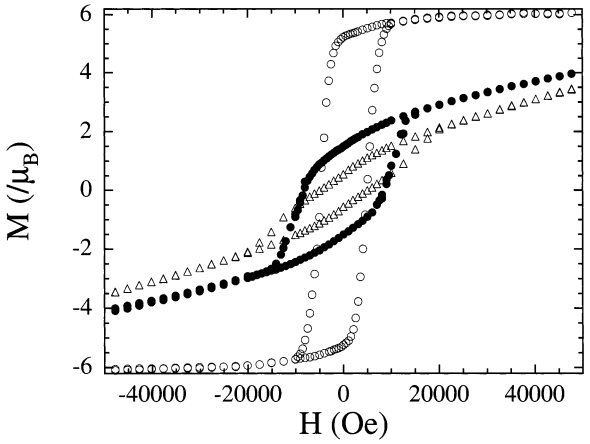

Figure 6. Field dependence of the magnetization at 1.8 K on oriented single crystals of **1** along the chains (○) perpendicular to the chains in the *ac* plane (●) and along the monoclinic *b* axis (△).

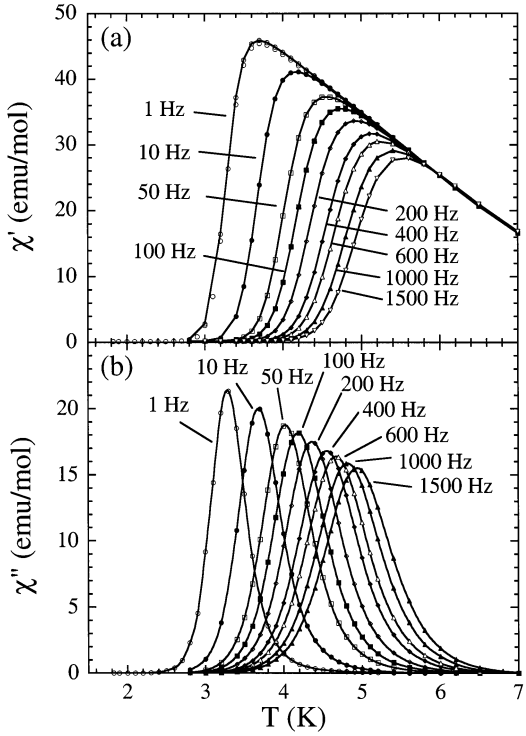

Figure 7. Temperature and frequency dependence of the (a) real (χ') and (b) imaginary (χ'') part of the ac susceptibility. The solid lines are guides.

at 10 K, the magnetization quickly saturates to the expected value of $6\mu_B$. The coercive field in this direction is 5000 Oe; a similar value is found on the polycrystalline sample.[24] Even if such a behavior is usually seen below a ferromagnetic or ferrimagnetic tridimensional ordering temperature, another possibility could be the occurrence of a frozen magnetized state. To prove this assumption, we have performed detailed alternating current (ac) magnetic measurements.

Below 6.5 K, the ac susceptibilities (χ' and χ'' are the real and imaginary components of the ac susceptibility, respectively) are strongly frequency dependent (Figure 7). Unambiguously, this result precludes any tridimensional ordering. Slow relaxation of the magnetization is directly responsible for this behavior in

(24) At 1.8, 2, 2.5, and 3 K, the coercive field is found to be 4500, 1500, 60, and 10 Oe, respectively, on polycrystalline sample of (**1**).

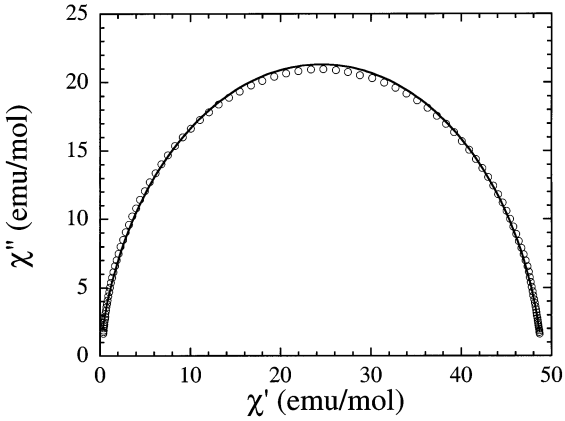

Figure 8. Cole−Cole diagram at 4 K. The solid line represents the least-squares fit obtained with a Debye model (see text).

SMM,[2,3] superparamagnetic,[25] or spin-glass[26] systems. When lowering the temperature, the decrease of χ' (Figure 7a), with the appearance of χ'' (which becomes different from zero between 6.5 K at 1500 Hz and 4.5 K at 1 Hz, Figure 7b), is directly associated to a blocking process of the magnetization. Indeed, the thermal energy is not sufficient to allow the magnetization to follow the ac field at a given frequency (ν). At this frequency, the motion of the entire magnetization becomes frozen below the blocking temperature (T_B). This induces (i) ac responses to vanish (Figures 5 and 7) and (ii) the magnetization to exhibit coercivity (Figure 6). At a fixed temperature, we obtain a semicircle Cole−Cole diagram (χ'' versus χ', Figure 8), as expected for a Debye model with a single relaxation time (τ).[27,28]

Experimentally, τ could be deduced from the maximum of the $\chi''(\nu)$ curve at a given temperature. In the same way, the plot of χ'' as a function of the temperature (Figure 7) at a fixed frequency gives a maximum at T_B, that is, for $\tau(T_B) = 1/(2\pi\nu)$.[28] In Glauber's theory, the thermal variation of τ is described by an Arrhénius law:

$$\tau(T) = \tau_0 \exp(\Delta/(k_B T)) \tag{8}$$

where τ_0 is a preexponential factor, and Δ is the energy barrier to reverse the magnetization direction. At T_B, eq 8 implies

$$\frac{1}{T_B} = -\frac{k_B}{\Delta}(\ln(2\pi\nu) + \ln(\tau_0)) \tag{9}$$

In Figure 9, we have plotted $1/T_B$ versus $\ln(2\pi\nu)$. The experimental data follow a linear variation, which confirms the

(25) Morrish, A. H. *The Physical Principles of Magnetism*; Wiley: New York, 1965. Bean, C.; Livingston, J. D. *J. Appl. Phys.* **1959**, *30*, 120S−129S.

(26) Mydosh, J. A. *Spin Glasses: An Experimental Introduction*; Taylor & Francis: London, 1993. Chowdhury, D. *Spin Glasses and Other Frustrated Systems*; Princeton University Press: New Jersey, 1986. Moorjani, K.; Coey, J. M. *Magnetic Glasses*; Elsevier: New York, 1984. Binder, K.; Young, A. P. *Rev. Mod. Phys.* **1986**, *58*, 801−976.

(27) Cole, K. S.; Cole, R. H. *J. Chem. Phys.* **1941**, *9*, 341. Boettcher, C. J. F. *Theory of Electric Polarization*; Elsevier: Amsterdam, 1952. Aubin, S. M.; Sun, Z.; Pardi, L.; Krzysteck, J.; Folting, K.; Brunel, L.-J.; Rheingold, A. L.; Christou, G.; Hendrickson, D. N. *Inorg. Chem.* **1999**, *38*, 5329−5340.

(28) In a Debye model, the ac susceptibility, $\chi_{ac}(\nu) = \chi'(\nu) + i\chi''(\nu)$, is given by the following relation:

$$\chi_{ac}(\nu) = \frac{\chi_{ac}(\nu \to 0)}{1 + i[2\pi\nu\cdot\tau(T)]}$$

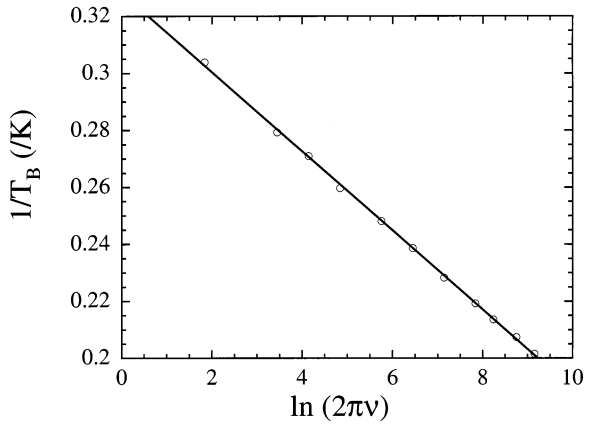

Figure 9. $1/T_B$ versus $\ln(2\pi\nu)$ plot. The solid line represents the least-squares fit of the experimental data to the Arrhénius equation (see text).

theoretical predictions. The best set of parameters obtained is $\tau_0 = 5.5(1) \times 10^{-11}$ s and $\Delta/k_B = 72(1)$ K.

These values mean that the relaxation time of the magnetization is on the order of 5 months at 1.8 K, allowing us to qualify this compound as a "magnet". It is worth noticing that the good crystallinity of the material (illustrating the absence of high disorder and crystallization solvents in the crystal packing), the lack of frustrated magnetic interactions, and the physically meaningful value of τ_0 and Δ preclude the spin-glass interpretation. As shown previously, the presence of ferromagnetic interactions between the trimer units along the chains also rules out the possibility of a SMM behavior and suggests a single-chain magnet behavior. Indeed, the slow relaxation of the magnetization in **1** is consistent with the mechanism proposed by Glauber for one-dimensional Ising systems. The preferential orientation of the magnetization is created by the combined effect of uniaxial anisotropy and local correlations promoting the parallel and antiparallel alignment of spin moments in the chain. The blocking process makes a tridimensional ordering impossible at lower temperature. Even if interchain interactions (J'') are present, the blocking energy barrier is too high to be overcome and to let the spin carriers be ordered between chains.

In Glauber's theory, the energy gap Δ should be equal to $4J'_{\text{eff}}$. Considering the J'_{eff} value deduced from the Ising fits (Figure 5), the expected value would be $\Delta_{\text{Glauber}}/k_B = 48$ K. This estimation is reasonable, although some discrepancy seems to exist beyond the experimental error. The same remark can be made concerning the results reported by A. Caneschi et al.[5] This suggests that Glauber's approach may be a relevant first approximation for real systems which present a large but finite anisotropy and/or very weak interchain coupling.

Concluding Remarks

In this paper, we report the synthesis, X-ray crystal structure, and magnetic properties of a unique one-dimensional heterometallic chain. This material exhibits a new fascinating magnetic behavior similar to the one predicted by Glauber for Ising-type chains. By analogy to the single-molecule magnets, this kind of material could be called a single-chain magnet. An important characteristic of our system is the high spin value of the magnetic unit inside the chain. The $S_T = 3$ ground state allows for a noticeable value of Δ (consistent with $\Delta_{\text{Glauber}} = 8S_T^2J'$) despite the small J' exchange ($J' \approx +0.7$ K). It is remarkable that with interunit couplings typically 100 times smaller than the one reported by A. Caneschi et al., we already obtain the same order of magnitude for the blocking temperature. Therefore, the use of high spin magnetic unit combined with strong interunit magnetic one-dimensional interactions appears to be an attractive route to design metastable magnets at high temperature. On the basis of this heterometallic one-dimensional chain of Mn^{III} and Ni^{II}, a new series of materials are currently under investigation. The substitution of transition metals as well as the use of different bulky ligands should help us to control the magnetic properties. This rational design of new one-dimensional architectures should allow for the tuning and the increasing of the blocking temperature.

Acknowledgment. R.C. and C.C. would like to thank the CNRS and the Conseil Regional d'Aquitaine for financial support. H. M. thanks the Japan Science and Technology Corp. (JST) for financial support.

Supporting Information Available: Crystallographic data for $[Mn_2(saltmen)_2Ni(pao)_2(py)_2](ClO_4)_2$ (CIF). This material is available free of charge via the Internet at http://pubs.acs.org.

JA0203115